GEOPHYSICAL RESEARCH LETTERS, VOL. 28, NO. 23, PAGES 4379-4382, DECEMBER 1, 2001

Slip distribution and tectonic implication of the 1999 Chi-Chi, Taiwan, Earthquake

Chen Ji[1], Donald V. Helmberger[1], Teh-Ru Alex Song[1], Kuo-Fong Ma[2], and David J. Wald[3]

Abstract. We report on the fault complexity of the large (M_w = 7.6) Chi-Chi earthquake obtained by inverting densely and well-distributed static measurements consisting of 119 GPS and 23 doubly integrated strong motion records. We show that the slip of the Chi-Chi earthquake was concentrated on the surface of a "wedge shaped" block. The inferred geometric complexity explains the difference between the strike of the fault plane determined by long period seismic data and surface break observations. When combined with other geophysical and geological observations, the result provides a unique snapshot of tectonic deformation taking place in the form of very large (>10m) displacements of a massive wedge-shaped crustal block which may relate to the changeover from over-thrusting to subducting motion between the Philippine Sea and the Eurasian plates.

Introduction

Located at the "corner" of convergence between the Philippine Sea and Eurasian plates (Fig.1), Taiwan results from the east-west (E-W) collision during the last 5 Ma [*Teng*, 1990]. Currently, southern Taiwan is still under intense collision due to the eastward subducting Eurasian plate underneath the Philippine Sea plate, but the tectonic style in northeast Taiwan reflects the northward subduction of the Philippine Sea plate beneath the Eurasian plate (e.g., *Teng et al.* [2000]). We expect that central Taiwan, where the 1999, Chi-Chi earthquake occurred, would contain a transfer zone where the convergence of subduction changes from E-W to N-S. The location of this transfer zone has not previously been resolved, presumably because of the complex surface geology in the Taiwan orogenic belt.

The Chi-Chi earthquake initiated at a depth of 10 km and ruptured the Chelungpu fault (CLPF) producing a 80 km long complex surface rupture pattern (*Kao and Chen* [2000], *Kao et al.* [2000]). The fault surface offsets increase from south to north with 7 m of vertical and over 8 m horizontal offsets observed (e.g., *Lee et al.* [2000]). While the GPS data indicate the existence of large northward oblique motion on the northern part of the fault (Fig. 1), the surface trace does not continuously follow the mapped CLPF, instead, it turns to the east and extends another 15 km striking N80E (Fig. 1). It is not obvious whether this extended piece of surface break is just a near-surface effect caused by slip on the CLPF, or corresponds to a large asperity on an unmapped fault. We address this question by modeling surface static displacement data following a finite fault approach [*Ji et al.*, 2001a], and try to constrain a reasonable fault geometry for the future study of the dynamic rupture.

Analysis

Observations in the vicinity of the surface rupture were selected, and include 119 GPS displacements and 23 doubly-integrated strong motion accelerograms (Fig.1, *Yu et al.* [2001]). Taken together, these data comprise one of the best static data sets yet recorded for finite analysis of a large earthquake. The inversions were performed on two finite fault model geometries. The first includes only one rectangular plane following the downdip extension of the portion of the CLPF that showed surface rupture. The second is composed of three planes that follow the strike of the three major segments of surface break (Fig. 1).

In contrast with the half-space earth model used in *Johnson et al.* [2001], here a more realistic layered earth model (Table-1, *Ma et al.* [1996]), is used to generated static response [*Xie and Yao*, 1989]. The apparent discrepancy between the vertical and horizontal observations noted by *Johnson et al.* [2001] can be explained by introducing a softer surface condition. For example, numerical tests show that for a pure thrust fault with 30 degree dip angles, the response generated by a half-space earth model will be up to 10% smaller than that of the layered model in the hanging wall and over 30% larger in footwall.

We employ a simulated annealing algorithm to find the global optimal solutions [*Ji et al.*, 2001a]. A series of inversions are performed to test the importance of fault dip-angles, essentially by grid searching all possible dip angles. For example, the error function is nearly constant when the fault dip of Fault-2 changes from 20^o to 30^o, but increases dramatically for other dip an-

[1],Seismological Laboratory, California Institute of Technology, Pasadena

[2], Institute of Geophysics, National Central University, Chung-Li, Taiwan

[3],U.S. Geological Survey, Pasadena

Paper number 2001GL013225.
0094-8276/01/2001GL013225$05.00

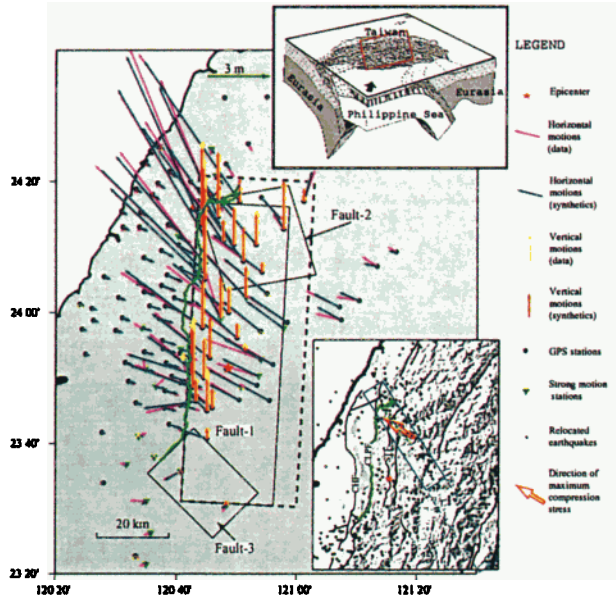

Figure 1. Upper-right inset shows the regional tectonic framework (Modified from *Angelier* [1986]); a red box is used to indicate the study region. The surface fault break is displayed as a heavy green line in the lower-inset along with topography map and the major faults (thin lines, CHF = Changhua fault; CLPF = Chelungpu fault; STF = Shuangtung fault; SLF = Shuli fault). The relocated small earthquakes during 1991-1993 [*Ma et al.*, 1996] are used to display the position of SanYi-Puli seismic zone (solid blue box). The trend of maximum compressional stress direction is 302 ± 22^o [*Hu et al.*, 1996]. Two fault models are displayed in the main figure. The first idealizes the entire event as a rectangle striking striking N3°E with a dimension (37 km by 95 km) (dashed line box). The second approximates the faulting with three faults: Fault-1 again striking N3°E, Fault-2 striking N80°E along the northern segment and Fault-3 striking N45°E along the southern segment. All fault segments dip 30° to the east. The synthetic displacements were generated from the second model.

gles. Sizes of the fault planes were also examined to insure enough elements. Figure 2 displays the final inversion results for the two assumed faulting geometries. The inversions indicated that, the single-plane model fits the data quite well, except at the two ends. With the optimum multi-plane model (Fig.2 a and b), we further reduced the total sum-squared error an order of magnitude over the single-plane model. Moreover, the slip pattern recovered by the optimum model suggests a very plausible physical rupture scenario. In Figure 2a, we plot the spatial distribution of the multi-plane solution. It appears that Fault-1 and Fault-2 cross each other and form the surfaces of a "wedge shaped" block. The intersection of two planes, or the margin (edge) of the block, extends from the free surface, where the fault break makes a nearly right angle turn, to the bottom of the planes, and is displayed in Figure 2b and 2c by a thick black line. Note that there is very little slip below this intersection boundary, while there are large displacements just above it. Such results are probably not an artifact produced by the inversion since our approach suppresses slip heterogeneity (*Ji et al.* [2001a]). Thus, the slip appears to be confined entirely to the "wedge" which produced a massive uplift as displayed in Figure 3. Note that the sense of slip on the wedge surface is fully compatible with the maximum stress direction as indicated in Figure 1. Moreover, this direction is in agreement with the trend of the P (compression) axis

Table 1. Central Taiwan Crustal Model

V_p (km/s)	V_s (km/s)	ρ (g/cm^3)	Th (km)	μ ($\times 10^{10} Nm^{-2}$)
3.50	2.00	2.0	1.0	0.8
3.78	2.20	2.3	3.0	1.1
5.04	3.03	2.5	5.0	2.3
5.71	3.26	2.6	4.0	2.8
6.05	3.47	2.6	4.0	3.1
6.44	3.72	2.6	8.0	3.6
6.83	3.99	3.0	5.0	4.8
7.28	4.21	3.0	0.0	5.3

V_p, V_s, ρ, th and μ are the P wave velocity, S wave velocity, density, thickness and rigidity of each layer, respectively.

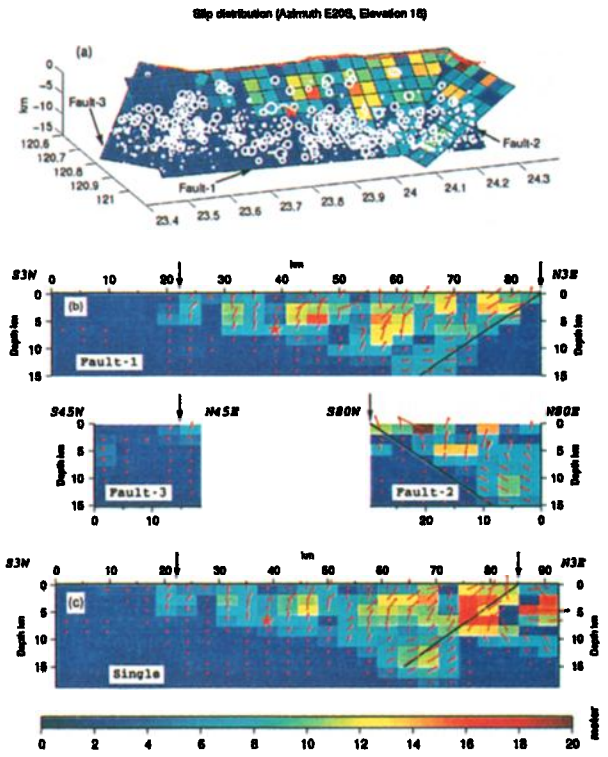

Figure 2. The top panel (a) displays the fault geometry for the multi-fault plane model with the main branch along the CLPF (Fault-1) and two secondary segments, Fault-2 and Fault-3. Plan views of these three faults are given in the second panel (b). The white circles show the aftershocks (Central Weather Bureau, Taiwan). The bottom panel (c) displays the results for a single-plane model. The color and arrows are used to indicate the slip amplitudes and directions. We have included a heavy dark line indicating the intersection points between Fault-1 and Fault-2. Note the absence of slip below this line in the multi-plane model and the rapid changes in the one-plane case in the vicinity of the boundary.

Table 2. Comparison of Fault Plane solutions

	Plane 1			Plane 2			P Axis	
	θ	δ	λ	θ	δ	λ	Az	Pl
Harvard	37	25	96	211	65	87	303	20
Combined	25	25	78	218	65	96	304	20
Fault-1	3	30	59	218	65	107	295	18
Fault-2	80	30	128	218	67	70	322	19
Single	3	30	57	220	65	107	297	18

θ, δ and λ are the strike, dip and rake angles, respectively. Az and Pl are the azimuth and plunge angles of P axis. The units of all values are degrees.

derived from the multi-plane model (Table 2), and the aftershock fault plane solutions [*Kao and Chen*, 2000]. The fault geometry and slip distribution are consistent with the work of *Johnson et al.* [2001], even though entirely different forward and inverse approaches were used. The smaller optimal dip angles ($20 - 25^o$) they reported are probably due to the half-space earth model used. The slip distribution is also similar to that estimated by teleseismic inversions *Ma et al.* [2000].

The multi-plane model explains the apparent disparity between the Harvard Centroid Moment Tensor (CMT) solution and the CLPF orientation (see Table-2). Note the strike of Fault-1 differs by more than 30^o from that derived from CMT. However, such a result is expected because the slip of the Chi-Chi event involved multiple fault planes. The CMT solution is primarily based on long period seismic waves with wavelengths over 300 km, hence the 80 km extent of this earthquake can be roughly approximated as a point source. The CMT solution, thus, reflected the vector summations of all contribution from the variable-geometry multi-fault segments. In Table 2, we show that the best double couple solution of the combined model is very close to the CMT solution.

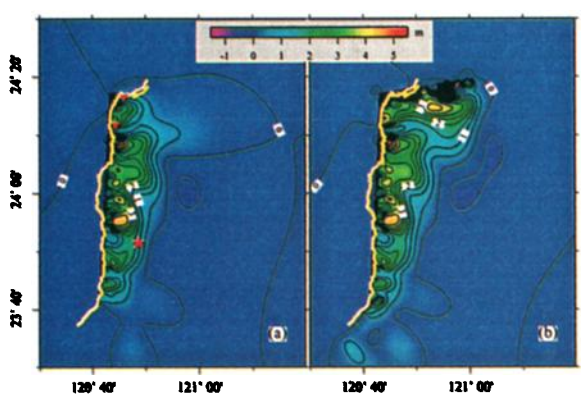

Figure 3. Uplift predictions at the surface produced by the multi-plane model with the contribution of Fault-1 on the left and the combined fault on the right. The motions are given in contours expressed in meters. The peak values reach about 5 m at the surface, and the total uplift volume is $2.4 \times 10^9 m^3$. Note that Fault-2 plays a major role in generating the static field at many northern stations. The triangles donated two strong motion stations used in Fig. 4.

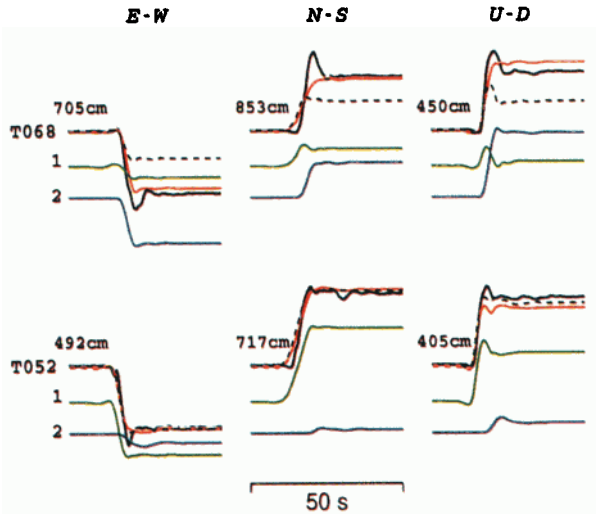

Figure 4. Comparison of observed strong motion displacements and synthetic seismograms at two stations, T052 (south) and T068 (north) as displayed in Figure 3. The black traces are data. The dashed traces were produced by the single-plane model and red by the combination of Fault-1 (green traces) and Fault-2 (blue traces). All the traces are aligned on the P-wave first arrivals and a rupture velocity of 1.9 km/s is required to produce such alignment (assuming the velocity model in Table-1). We assume that all elements have the same rise-time function with a width of 7.5 s.

Since our solution is mainly controlled by numerous GPS measurements, one might wonder if some of this slip occurred during the numerous large aftershocks [*Kao and Chen*, 2000]. We address this issue by computing the dynamic solution with our static models. For each point on the multi-fault plane, we define its rupture distance as the shortest on-fault-plane distance from the hypocenter, and its rupture initiation time is assumed to be the ratio of the rupture distance to the average rupture velocity along the shortest distance path. Then the seismic waveforms at two strong motion stations at the northern end (Fig. 3), where the largest GPS motions were observed, can be simulated very well with the multi-plane slip model and very simple assumptions of the rise time and the rupture velocity (Fig. 4). Note the displacement at T068 (the northern station) is dominated by the contribution of Fault-2, whereas, the contribution of Fault-1 dominates the displacement of T052. While the single-plane model solution can explain the waveforms of station T052 equally well, it fails to model those at station T068, even though these stations are less than 10 km apart. Further research will be directed toward a combined inversion of seismic and geodetic data with the inverted fault geometry. That will help us to clarify this question.

Discussion

It appears that motions of two major fault planes of the Chi-Chi earthquake exhibit mechanical characteristics similar to the larger scale interaction between

two plates. The CLPF and two adjacent faults to the east, the Shuang-Tung fault (STF) and the Shu-Li fault (SLF), formed by the east-west collision between the two plates [*Teng*, 1990], either turn to the east or are truncated by the east-west trending valley near their northern ends (Fig. 1, lower-inset). The surface projection of the hinge axis (green dashed line in Fig. 1) of the Chi-Chi earthquake rupture surface appears to connect the bending or truncation points of the two other faults. Fault-2 and the northern ends of the two other faults seem to form a thrust belt that migrates to the northwest and intersects with the older south-north striking thrust faults as the subduction of the Philippine Sea plate continued. Furthermore, a linear seismic zone (the Sanyi-Puli seismic zone, lower-inset of Fig. 1) also follows the trend of the hinge axis and small earthquakes are concentrated on northeast side of the zone where the new faults, like Fault-2, are forming. Finally, the southeast extension of the Sanyi-Puli seismic zone meets with the coastal line at approximately 23.4°N. This point roughly separates the coastal region into two domains. The geophysical observations in the southern domain indicate strong crustal shortening, deep seismicity and positive offshore free-air gravity anomalies, reflecting the existence of a deep subducted Eurasian slab. Observations in the northern domain show small component of crustal compression, shallow but strong seismicity and large negative offshore gravity anomalies, suggesting that in this region, the Philippine Sea plate has already started to subduct beneath the Eurasian plate (e.g., *Chemenda et al.* [1997]). Hence, the hinge in the "wedge" shape occurring in the Chi-Chi rupture surface may mark the present position of the transfer zone where the change in subduction polarity occurs.

The rupture pattern produced by this event involving old and new faults, similar to other recent studies (e.g., the 1992 Landers earthquake, *Nur et al.* [1993]; the 1999 Hector Mine earthquake, *Ji et al.* [2001b]), is related to evolutionary stress conditions and may provide unique information pertaining to the spatial and temporal patterns of tectonic processes.

Acknowledgments

We particularly thank S.-B. Yu for offering the GPS observations, M. Simons, J. Saleeby and two anonymous reviewers for comments on this manuscript. This work is supported in part by SCEC contract No. NSF EAR-8920136 and by the U.S.geological Survey under Contract No. 1HQGR0098. Contribution No. 8838, Division of Geological and Planetary Sciences, California Institute of technology, Pasadena, California 91125.

References

Angelier, J., Geodynamics of the Eurasia-Philippine Sea Plate boundary: Preface, *Tectonophysics*, *125*, 1–3, 1986.

Chemenda, A. I., R.-K. Yang, C.-H. Hsieh, and A. L. Groholsky, Evolutionary model for the Taiwan collision based on physical modeling, *Tectonophysics*, *274*, 253–274, 1997.

Hu, J.-C., J. Angelier, J. Lee, H.-T. Chu, and D. Byrne, Kinematics of convergence, deformation and stress distribution in the Taiwan collision area: 2-D finite-element numerical modelling, *Tectonophysics*, *255*, 243–268, 1996.

Ji, C., D. J. Wald, and D. V. Helmberger, Source description of the 1999 Hector Mine, California earthquake; Part I: Wavelet domain inversion theory and resolution analysis, *Bull. Seism. Soc. Am.*, *Submitted*, 2001a.

Ji, C., D. J. Wald, and D. V. Helmberger, Source description of the 1999 Hector Mine, California earthquake; Part II: Complexity of slip history, *Bull. Seism. Soc. Am.*, *Submitted*, 2001b.

Johnson, K. M., Y.-Y. Hsu, P. Segall, and S.-B. Yu, Fault geometry and slip distribution of the 1999 Chi-Chi, Taiwan earthquake imaged from inversion of GPS data, *Geophys. Res. Lett.*, *28*(11), 2285–2288, 2001.

Kao, H., and W.-P. Chen, The Chi-Chi Earthquake sequence: Active, out-of-sequence thrust faulting in Taiwan, *Science*, *288*, 2346–2349, 2000.

Kao, H., R.-Y. Chen, and C.-H. Chang, Exactly where does the 1999 Chi-Chi earthquake in Taiwan nucleate? -Hypocenter relocation using the Master station method, *TAO*, *11*(3), 567–580, 2000.

Lee, Y., Y. Sugiyama, T. Azuma, and Y. Kariya, Displacement and segmentation of the surface fault, 1999 Chi-Chi , Taiwan, Earthquake, *EOS*, p. F882, 2000.

Ma, K.-F., J.-H. Wang, and D. Zhao, Three-dimensional seismic velocity structure if the crust and uppermost mantle beneath Taiwan, *Journal of Physical Earth*, *44*, 85–105, 1996.

Ma, K.-F., S.-J. L. Teh-Ru Alex Song, and H.-I. Wu, Spatial slip distribution of the September 20, 1999, Chi-Chi, Taiwan, earthquake (M_w 7.6)–Inverted from the teleseismic data, *Geophys. Res. Letters*, *27*(20), 3417–3420, 2000.

Nur, A., H. Ron, and G. C. Beroza, The nature of the Landers-Mojave earthquake line, *Science*, *261*, 1993.

Teng, L. S., Geotectonic evolution of late Cenozoic arc-continent collision in Taiwan, *Tectonophysics*, *183*, 67–76, 1990.

Teng, L.-S., C.-T. Lee, Y.-B. Tsai, and L.-Y. Hsiao, Slab breakoff as a mechanism for flipping of subduction polarity in Taiwan, *Geology*, *28*, 155–158, 2000.

Xie, X.-B., and Z.-X. Yao, A generalized reflection-transmission coefficient matrix method to calculate static displacement field of a dislocation source in a stratified half-space, *Chinese J. Geophysics*, *32*, 191–205, 1989.

Yu, S.-B., et al., Preseismic deformation and coseismic displacements associated with the 1999 Chi-Chi, Taiwan Earthquake, *Bull. Seism. Soc. Am.*, *submitted*, 2001.

Chen Ji, Donald V. Helmberger and Teh-Ru Alex Song, Seismo Lab 252-21, Caltech, Pasadena, CA 91125, U.S.A. (e-mail: jichen@gps.caltech.edu)

Kuo-Fong Ma, Institute of Geophysics, National Central University, Chung-Li, 320-54 Taiwan

David J. Wald, U.S. Geological Survey, 525 South Wilson Avenue ,Pasadena, CA 91106, U.S.A.

(Received 03/26/01; revised 07/03/01; accepted 09/05/01.)